PAPER • OPEN ACCESS

Kinematics and shear-induced alignment in confined granular flows of elongated particles

To cite this article: Antonio Pol *et al* 2022 *New J. Phys.* **24** 073018

New Journal of Physics
The open access journal at the forefront of physics

Deutsche Physikalische Gesellschaft DPG
IOP Institute of Physics

Published in partnership with: Deutsche Physikalische Gesellschaft and the Institute of Physics

OPEN ACCESS

RECEIVED
24 February 2022

REVISED
21 June 2022

ACCEPTED FOR PUBLICATION
30 June 2022

PUBLISHED
14 July 2022

PAPER

Kinematics and shear-induced alignment in confined granular flows of elongated particles

Antonio Pol[1,2,*], Riccardo Artoni[2], Patrick Richard[2], Paulo Ricardo Nunes da Conceição[3] and Fabio Gabrieli[1]

[1] Department of Civil, Environmental and Architectural Eng. (ICEA), Università degli Studi di Padova, Via Ognissanti 39, 35129 Padova, Italy
[2] MAST-GPEM, Université Gustave Eiffel, F-44344 Bouguenais, France
[3] Mineral Processing Laboratory, Federal University of Rio Grande do Sul (UFRGS), Brazil
[*] Author to whom any correspondence should be addressed.

E-mail: antonio.pol@univ-eiffel.fr

Keywords: particle shape, granular flows, orientational order, rotational dynamics

Abstract

The kinematics and the shear-induced alignment of elongated particles in confined, heterogeneous flow conditions are investigated experimentally. Experiments are conducted in an annular shear cell with a rotating bottom wall and a top wall permitting confinement of the flow. Flow kinematics and particle orientation statistics are computed by particle tracking using optical imaging. Translational velocity profiles show an exponential decay, and surprisingly, only the slip velocity at the bottom is influenced by the particle shape. Rotations are highly frustrated by particle shape, more elongated particles showing, on average, a lower angular velocity. In addition, a clear shear-rate dependency of the proneness of a particle to rotate is observed, with a stronger inhibition in low shear zones. The average orientation of the particles does not correspond to the main flow direction, they are slightly tilted downwards. The corresponding angle decreases with the particles' elongation. Orientational order was observed to increase with particles' elongation, and surprisingly was not affected by the applied confinement. A weak but systematic decrease of the orientational order was observed in regions of higher shear rate. At the particle-scale, angular velocity fluctuations show a strong correlation with local particle orientation, particles being strongly misaligned with the preferential particles' orientation rotating faster. This correlation becomes stronger for more elongated particles, while is almost unaffected by the applied confinement.

1. Introduction

Granular materials are often composed of particles with anisotropic shapes, like rice, lentils or pills. Yet, for the sake of simplicity, the majority of the experimental and theoretical studies have focused on spherical particles. In recent years, several works have shed light on the peculiar behaviour induced by the shape anisotropy of the particles. Among them one can mention the effects in the packing fraction of granular packings [1–3], stresses in piles [4–8], the average coordination number [9] or the jamming [10, 11]. Also, it has been shown that the particles' shape has a significant effect on the global response of the granular material when submitted to an external mechanical solicitation like taps [12–16] or shear [7, 8, 17–19]. Thus, it turns out that the particles' shape has a remarkable influence on the behaviour of granular media, and can introduce qualitatively new macroscopic phenomena with respect to the case of shape-isotropic grains. An overview of the behaviour of granular media composed of shape-anisotropic particles is given in Börzsönyi and Stannarius [20].

In this work, we focus on granular materials made of elongated particles and continuously submitted to shear. Such type of systems are strongly influenced by the shape anisotropy of the particles: they show collective reorientation under shear and shear-induced orientational ordering. The latter phenomenon is

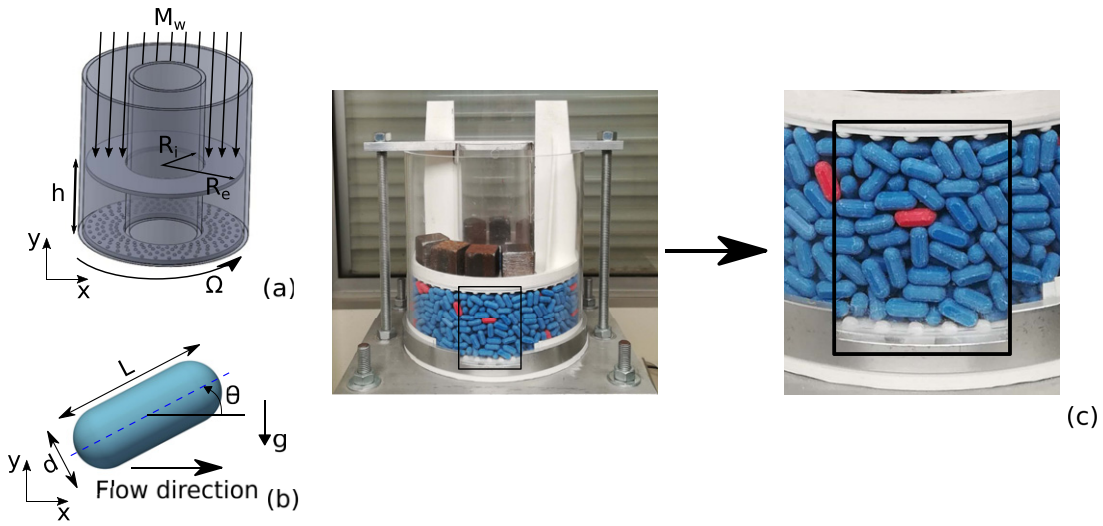

Figure 1. (a) Sketch of the annular shear cell, the top wall imposes a load M_w on the granular material and the bottom wall rotates with a velocity Ω. (b) Geometry of a spherocylinder of length L and diameter d. Its orientation with respect to the flow direction is characterised by the angle θ (in the x–y plane). (c) View of the experimental cell with a particular of the monitored region (black rectangle).

robust and has been observed in different configurations as shear flows [18, 19, 21–27], flow down an inclined plane [25, 28] and hopper flows [29–32]. In a recent work Artoni and Richard [27] suggested that the correlation between angular velocity fluctuations and local particle orientation is at the base of the orientational ordering in shape-anisotropic granular media. In granular flows particles that are strongly misaligned with the streamlines rotate quicker, on an average basis, than particles aligned with the flow direction. This is similar to the motion of isolated elongated bodies in a viscous flow [33]. However, due to the entanglement between particles in a granular system, the average dependence of angular velocity on the orientation may be stronger than the one predicted by Jeffery's model [33].

Previous research on the rotational dynamics of elongated particles in granular flows has focused on heterogeneous free surface shear flows [23, 24]. Here we add the further constraint of a vertical confinement to the flow. Wall-bounded shear flows, are often characterised by complex localisation patterns [34–36], and qualitatively and quantitatively different behaviours are observed between the zones characterised by low shear rate and the zones in which large shear is localised. Therefore, in this work, we focus on elongated particles in highly confined heterogeneous shear flows, trying to understand how shear heterogeneity and flow confinement influence particles rotational dynamics and their orientational ordering.

The paper is organised as follows. The experimental methodology is presented in section 2. In section 3, we report the kinematic properties of our flow, i.e. the translational and rotational velocity profiles. Section 4 is devoted to the study of the orientational order of the particles. In section 5, we present a detailed discussion on the correlation between orientation and angular velocity. Finally in section 6 we summarise our findings.

2. Experimental methodology

2.1. Experimental setup

Experiments were conducted in an annular shear cell geometry [35, 37] filled with spherocylindrical particles (see figure 1). The shear cell is composed by two vertical and coaxial cylindrical walls made of poly-methyl methacrylate (PMMA). The internal radius of the outer cylinder is $R_e = 95$ mm and the external radius of the inner cylinder is $R_i = 45$ mm, therefore the inner annular region is 50 mm thick. The horizontal boundaries are two annular walls made of poly-lactic acid (PLA) obtained through 3D printing. The top and bottom horizontal walls have a bumpy surface characterised by a triangular mesh of hemispheres (diameter $b = 6$ mm) with a mean distance of $2b$ between their edges. The bottom plate is screwed to a rotating plate driven by a stepper motor (Lexium MDRive, Schneider Electric). The top plate is connected to a support preventing its rotation but permitting it to freely move vertically. Steel masses can be placed on the top plate in order to apply a vertical load on the granular medium. The spherocylindrical particles are 3D printed in order to control their shape and material (PLA). Moreover, the 3D printing also

Table 1. Summary of the experimental combinations. The parameter M^* is the ratio between the applied mass M_w over the total mass of the particles M_g. AR is ratio of the spherocylinder's length L to its diameter d.

AR (−)	M_g (kg)	M_w (kg)	M^* (−)
2.0	0.93	0.67	0.7
2.0	0.93	1.94	2.1
2.0	0.93	3.64	3.9
2.5	0.93	0.67	0.7
2.5	0.93	1.94	2.1
2.5	0.93	3.64	3.9
3.0	0.93	0.67	0.7
3.0	0.93	1.94	2.1
3.0	0.93	3.64	3.9

allows us to choose the particles' color. A 5% in mass of the total amount of particles was printed with a red color in order to use these particles as tracers for particle tracking.

Three sets of particles characterised by a different aspect ratio AR (= 2, 2.5, 3), i.e. ratio of the spherocylinder's length L to its diameter d (see figure 1(b)), were considered. The particle diameter d is 6 mm, independently of the AR considered. The total amount of particles is $M_g = 0.93$ kg, which corresponds to a flow height h of ∼72 mm (∼12d). In all the experiments here presented a rotational velocity of $\Omega = 5.86$ r.p.m. was imposed to the bottom wall. The bottom wall velocity was not changed in our study since Artoni *et al* [27] have shown that the shape of the kinematic profiles is not influenced by the bottom wall velocity in the adopted confined flow configuration. Furthermore, in a free surface flow configuration, Börzsönyi *et al* [23, 24] have shown that the average particles' alignment is essentially independent of the shear rate. Three different top loads were used for each of the AR considered imposing a weight $M_w = 0.67, 1.94, 3.64$ kg. The applied load will be indicated with the dimensionless parameter $M^* = M_w/M_g$ in what follows. The combinations of load and AR here investigated are summarised in table 1.

2.2. Measurement of the flow kinematics

The flow process was recorded with an industrial CMOS camera (Basler acA2440-75uc) and a light-emitting diode lamp was used for lighting the system. The control region (black rectangle in figure 1(c)) spanned the entire height of the flow and was 60 mm wide (∼10d). Given the wide span of velocity values in the flow, multiple movies were recorded at two different frame rates. Four 1 h long movies at 10 fps and two 6 h long movies at 1 fps were recorded for each of the parameter combinations reported in table 1.

A particle tracking algorithm (PTA) was used to reconstruct the kinematic profiles of the flow. Tracers particles (i.e. red particles) are identified using a color-based filter. Identified contours are filtered on the basis of threshold values of their surface and aspect ratio to discard contours that are not clearly associated with a single particle, as for instance spherocylinders not aligned with the wall of the cell (less than 20% of the spherocylinders was not aligned with the wall of the cell), or red spherocylinders that get stuck to each other. Finally, short trajectories, i.e. shorter than five frames long, are also discarded. In order to compute particles' rotation and orientation, in the PTA we find the best fitting ellipse (in a least-squares sense) of the recognised tracers' contour (see figure 2). Then, the angle θ between the long axis of the ellipse and the flow direction, in the x–y plane (x being the direction of the flow and y the direction along with gravity acts), is used to estimate the particle's orientation ($-90^\circ \leqslant \theta \leqslant 90^\circ$); the rotational velocity is therefore computed as the variation of the particle's orientation between consecutive frames. It should be noted that the optical measurements only permit the statistics of the particles at the wall to be computed, which may differ from the one characteristic of the particles in the bulk region. However, due to the limited width of the flow (<10d), one can reasonably assume that transverse gradients (with respect to the flow direction) are small and, therefore the quantities in the bulk should not substantially differ from the ones characteristic of the particles at the wall. Comparison between experiments repetitions highlighted that they were fairly repeatable. No relevant variation of the global packing fraction was observed between the different cases here analysed.

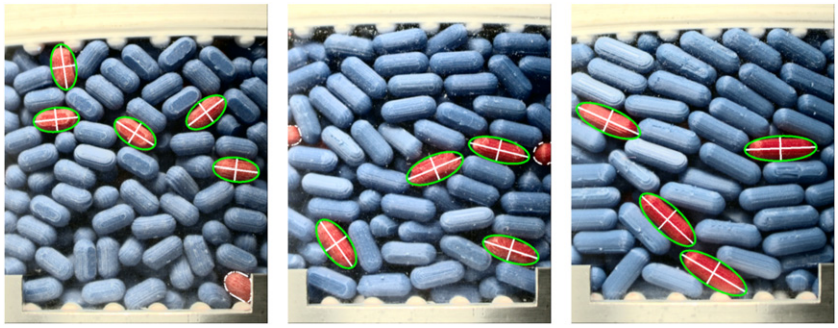

Figure 2. Examples of particles recognition in the particle tracking algorithm: AR = 2 (left), AR = 2.5 (centre), AR = 3 (right).

3. Kinematic profiles

In the following, we present the effect of the particles' elongation and of the top wall load on translational and rotational velocity profiles. All the profiles presented in this section refer to time averaged variables. Due to the non homogeneity of the flow, both the shear rate and the inertial number are not constant. The typical range of shear rate observed in the experiments is $10^{-2} < \dot{\gamma} < 1$, where lower values refer to the top region of the flow and the higher to the zone of shear localisation at the bottom of the flow. The inertial number instead, globally ranges between $I = 10^{-5}$ and $I = 10^{-2}$ (the inertial number was computed using the definition proposed by Hidalgo *et al* [28] for nonspherical particles). Given that the effects of the particles' elongation and of the top wall load were found to be independent, we discuss them independently, by showing variations with respect to the intermediate base case (AR = 2.5, $M^* = 2.1$). The velocity profiles obtained for the experiments with particles of AR = 2.5 are reported in figure 3(a). They show an exponential decay with the vertical position y, with a shear localisation near the bottom wall, which can be represented by the following equation:

$$v(y) = (V_w - v_{slip}) \exp\left(-\frac{y}{\delta}\right), \tag{1}$$

where $V_w = \Omega(R^e - b/2)$ is the azimuthal velocity of the bottom wall asperities closest to the transparent wall, and v_{slip} is the slip velocity at the bottom wall. The decay of the profile, i.e. δ, is influenced by the applied load with a strengthening of the flow localisation when increasing the latter. This flow behaviour is analogous to the one observed for spherical particles in a similar test configuration [35, 37]. Velocity profiles obtained for different aspect ratios are reported in figure 3(b).

A higher slip velocity is observed when considering particles characterised by a higher AR; this may be due to the lower relative dimension of the wall's asperities with respect to the major axis of the particles, i.e. b/L, for more elongated particles. However, once scaled by the velocity at the base of the flow, the velocity profiles obtained at different AR collapse on a single curve as highlighted in the inset of figure 3(b). Therefore, the decay of the velocity profiles seems independent of the particle elongation. Moreover, it means that the flow heterogeneity is the same for the three aspect ratios considered here.

The angular velocity profiles (here counterclockwise rotations are considered as positive) obtained for the experiments are reported in figures 4(a) and (b), considering the effect of the vertical confinement and of the particles aspect ratio respectively. It is evident that the angular velocity is strongly affected by the particle's shape (see figure 4(b)), the average particle's spin being systematically lower for higher AR (the range of $\dot{\gamma}$ is independent of AR). This agrees with the numerical observations of Artoni & Richard [27] in a 2D simple shear flow configuration. A variation of the vertical load has instead an almost negligible effect on the angular velocity with only slightly lower values for the higher vertical confinements (see figure 4(a)); however, the observed differences are compatible within the error bars.

For isotropic particles in homogeneous shear flows, the average particle angular velocity is not an independent variable, but is enslaved to the vorticity of the flow, and is given by half of the shear rate. Deviation from this scaling may arise due to the shape anisotropy of the particles, but also to the confined nature of the system that causes flow heterogeneity. It is therefore interesting to investigate the angular velocity normalised with the average shear rate at the location of the particle. In the insets of figures 4(a) and (b), the normalised angular velocity profiles are displayed. For shape isotropic frictional particles, the relation $\omega = -\dot{\gamma}/2$ has been observed, both in 2D and 3D numerical simulations and in different flow configurations [27, 38–42]. Instead, in our experiments we observe that $\omega' = -\omega/\dot{\gamma}$ is systematically lower

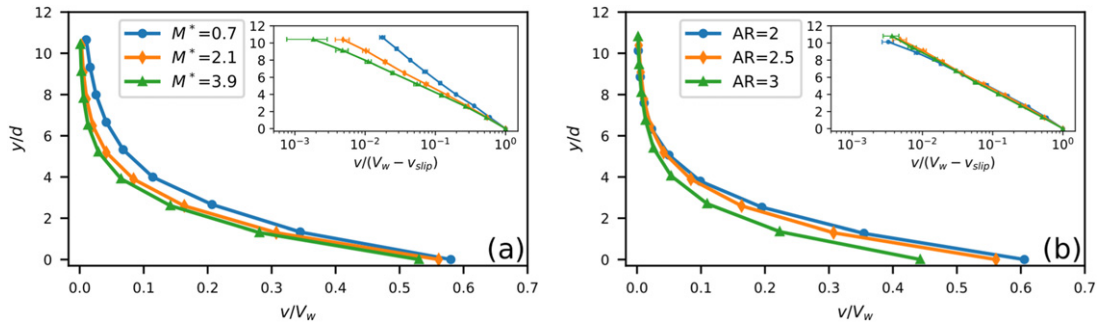

Figure 3. Time averaged translational velocity profiles: (a) effect of the vertical load M^* (AR = 2.5), (b) effect of the aspect ratio AR ($M^* = 2.1$). Velocity is normalised by the wall velocity V_w. The error bars are smaller than the size of the data markers. The insets report the velocity profiles normalised by the $V_w - v_{slip}$ in log-lin scale.

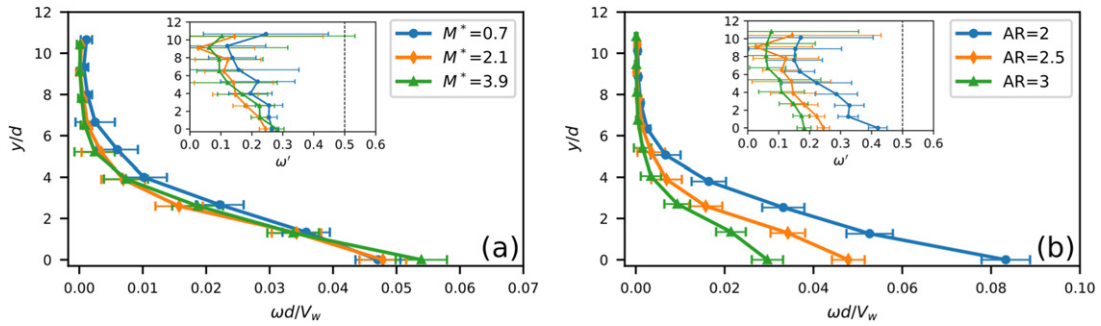

Figure 4. Time averaged angular velocity profiles: (a) effect of the vertical load M^* (AR = 2.5), (b) effect of the aspect ratio AR ($M^* = 2.1$). Angular velocity is normalised by V_w/d. The insets report the angular velocity profiles normalised by the local shear rate $\dot{\gamma}$ (the black-dashed line represents the expected value for isotropic particles [27, 38–42]).

than 0.5, independently of the considered aspect ratio and of the flow region. This reveals that there is a geometric frustration of the particles' rotation due the shape anisotropy of the particles.

Remarkably, ω' progressively decreases when moving farther from the zone of shear localisation (bottom region of the flow). This peculiar behaviour, which is not expected for spherical particles, underlines a further frustration of the particles rotation in systems made of shape anisotropic particles, which may be due to the combined effect of the confined nature of the flow and the higher orientational order in the zones characterised by a lower shear rate (the latter aspect will be detailed in section 4). In fact, differently from a spherical particle, the rotation of an elongated particle requires a local rearrangement of the neighbouring ones, and, in our confined flow, this rearrangement may be inhibited by both the vertical confinement and a more ordered phase. In our flow configuration, such inhibition becomes stronger when approaching the top wall and this may explain the decrease of ω' with y observed in the experiments. We observe a systematic decrease of ω' when increasing the particles AR (see the inset of figure 4(b)), which confirms the existence of a geometrical inhibition of particles rotations due to the shape anisotropy. Furthermore, a systematical decrease of the mean value of the normalised angular velocity $\overline{\omega'}$ with the particles aspect ratio is observed as displayed in figure 5(a). Finally, the normalised angular velocity ω' is displayed in figure 5(b) as a function of the shear rate $\dot{\gamma}$. It is noteworthy that, on an average basis, the proneness of a particle to rotate is strongly shear rate dependent. On the other hand the evolution of $\omega/\dot{\gamma}$ seems, surprisingly, to be nearly independent of the load, at least in the range studied here.

The inhibition of particles rotations is stronger for low shear rate values, while particles' rotation is less frustrated in zones where shear is localised. This is a new and very interesting result. We expect that this is strongly related to the development of solid fraction profiles. The medium is expected to be less dense in regions characterized by a higher shear rate; therefore, particles' entanglement is weaker in such regions and this could yield to a reduction of the frustration of particles' rotations. Previous works on free surface heterogeneous shear flows [23, 24] did not assess the dependence of ω' on the shear rate. While other flow features (e.g. particle orientation) are not or only slightly affected by the heterogeneity of the flow, in our case clearly the rotational frustration increases when moving towards low shear zones. The fact that such a behaviour was not pointed out before may be related to the highly confined nature of our flow. Finally, it

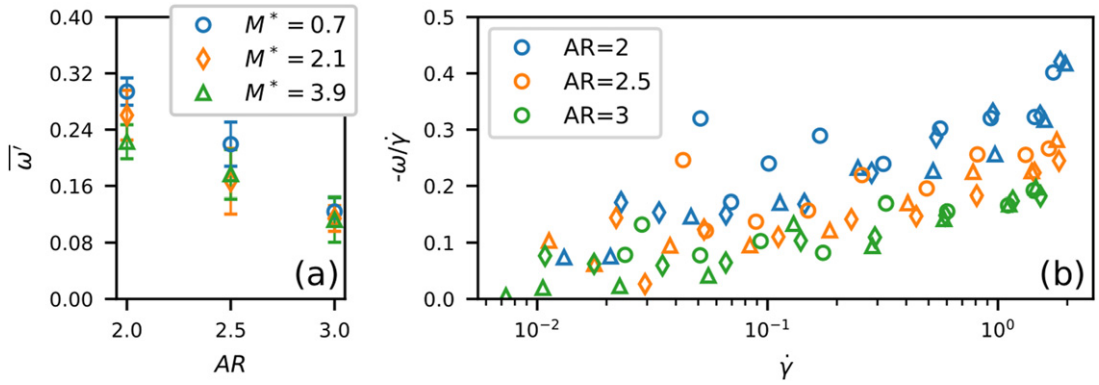

Figure 5. (a) Normalised average angular velocity $\overline{\omega'}$ as a function of the particles AR. (b) Normalised angular velocity as a function of the shear rate $\dot{\gamma}$. The confinement level is indicated with different symbols: $M^* = 0.7$ (○), $M^* = 2.1$ (◇), $M^* = 3.9$ (△).

should be noted that the data in figure 5(b) interestingly suggest the existence of a characteristic time. This aspect will be analysed in a future work.

4. Orientational order and alignment of the particles

In order to study the shear-induced alignment of the particles, their orientational distribution is considered at first. The orientation of a particle is defined as the angle θ between its long axis and the flow direction (see figure 1(b)). The orientational distribution is displayed in figure 6(a) for the cases with AR = 2.5 and different confinements, while the cases characterised by a different AR are compared in figure 6(b) with reference to a vertical load $M^* = 2.1$. For all the cases here considered, the distribution of θ is strongly anisotropic, and particles tend to be oriented, on average, with a non-zero angle with respect to the flow direction. In agreement with previous works [19, 21–24, 27], we observe that the distribution of θ is narrower when increasing the aspect ratio of the particles (see figure 6(b)). There is therefore a higher degree of shear-induced alignment in systems composed by more elongated particles. Surprisingly, minor differences are instead observed when modifying the vertical confinement, the only effect being a slightly more peaked distribution for higher confinement level (see figure 6(a)).

The average orientation θ_{av} of the particles with the flow direction is obtained by computing the circular mean. The values of θ_{av} as a function of the particles' aspect ratio are displayed in figure 7(a), for all the experimental combinations here considered. A systematic decrease of the misalignment between the average particles' orientation and the flow direction is observed when increasing the particles' elongation. Conversely, the average particles' orientation is almost unaffected by the applied vertical confinement. Finally, it is worth mentioning that the obtained θ_{av} values are consistent with the ones measured in free surface shear flows [23, 24] which, together with the independence of the vertical confinement, remarkably underlines the robustness of shear-induced alignment in granular media made of shape anisotropic particles. This suggests that the shear-induced alignment is mainly controlled by the particles' geometry (a slightly dependency on the particle friction has been observed in [43]) and seems almost independent of the flow configuration. This is an interesting perspective and should be investigated in a future work.

When analysing the distribution of the particles orientation, it has been observed that when using higher ARs the distribution becomes narrower. This already provided a first indication of the higher packing ordering that can be reached for more elongated particles. To provide a quantitative description of the shear-induced orientational order in our granular system we adopt the orientational order parameter S:

$$S = \langle 2\cos^2(\theta - \theta_{av}) - 1 \rangle, \tag{2}$$

where the average is made on all the particles having passed in a given zone at different times. In a perfectly ordered system the order parameter is equal to 1, while for a randomly oriented system the order parameter is equal to 0.

The order parameter S as a function of the aspect ratio of the particles is displayed in figure 7(b). Overall, we note a systematic increase of S with the aspect ratio of the particles. This tendency of reaching a higher orientational order in systems composed by more elongated particles is consistent with numerical results obtained in sheared granular systems composed of 2D dumbbells [21], elongated rods [18, 44], long

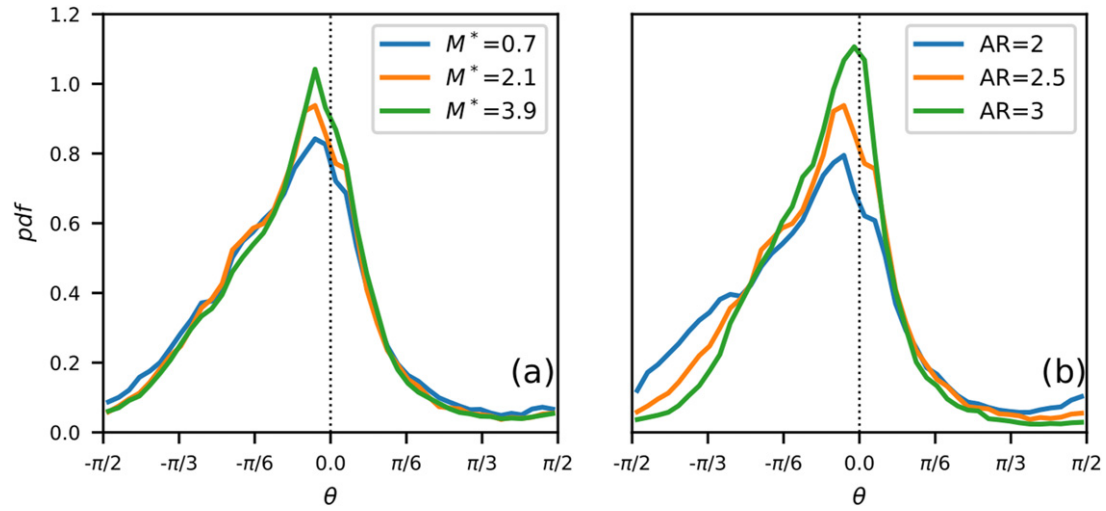

Figure 6. (a) Distribution of the particles' orientation θ: (a) effect of the vertical load M^* (AR = 2.5) and (b) effect of the aspect ratio AR ($M^* = 2.1$).

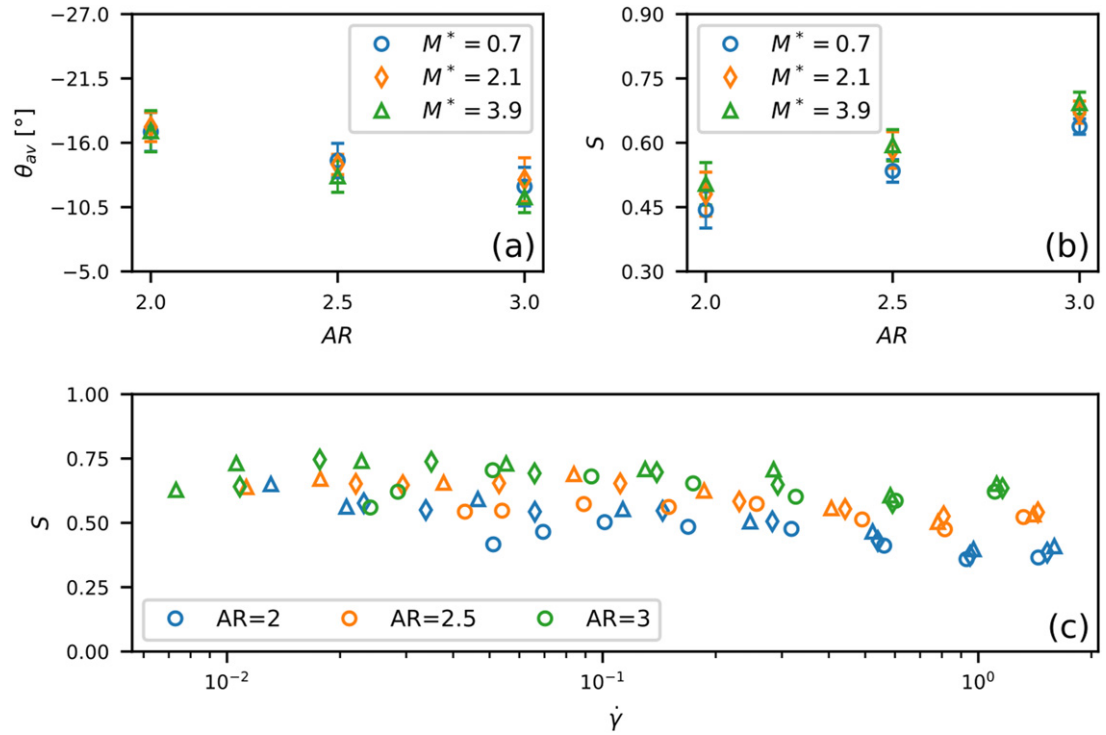

Figure 7. (a) Average orientation angle θ_{av} and (b) order parameter S as a function of the particles' aspect ratio AR. (c) Order parameter S as a function of the shear rate $\dot{\gamma}$. The confinement level is indicated with different symbols: $M^* = 0.7$ (○), $M^* = 2.1$ (◇), $M^* = 3.9$ (△).

clumps of overlapping spheres [23, 24], ellipses [26], ellipsoids [45] and spherocylinders [19, 43, 45], as well as with experimental results obtained with rice grains and rod like particles [23, 24].

Comparing the values of the order parameter for a given AR we observe that the effect of the applied confinement is almost negligible. Slightly less ordered phases are observed when applying a lower confinement, however the values of S are compatible within the error bars (see figure 7(b)). Finally, a weak dependency of the order parameter S on the shear rate is observed (see figure 7(c)). Indeed, a slight but systematic tendency of having more ordered states is observed in low shear rate zones, while a less ordered structure characterises the region of shear localisation.

5. Correlation between orientation and angular velocity

In order to investigate the correlation between angular velocity and local particle orientation, we perform a bin averaging on the orientation angle of the locally normalised angular velocity ω'. This yields a function ω'_θ, which represents the average angular velocity as a function of the orientation. The function ω'_θ is displayed in figures 8(a) and (b), where the effect of the applied confinement and of the particle aspect ratio can be observed.

Differently from the case of isotropic particles, for which the angular velocity is independent of the particle's orientation, we observe that, on an average basis, the angular velocity and the orientation are strongly correlated. Particles that are strongly misaligned with the average orientation θ_{av} tend to rotate faster, while particles oriented closer to θ_{av} rotate much slower. In the range $-15^\circ \leqslant \theta \leqslant 15^\circ$ particles rotate clockwise or counterclockwise with almost equal probability, and therefore the function ω'_θ is approximately equal to zero in such range of orientations. For higher misalignment with the flow direction, particles are mostly rotating in counterclockwise direction. Similarly to other works [24, 27], the angular velocity ω'_θ is maximum, on an average basis, for orientations orthogonal to the average particle orientation. We note that, as observed in [24], for particles oriented as $\theta_{av} \pm \pi/2$ the average angular velocity tends to the local vorticity of the flow. The ω'_θ is influenced by the particles AR (see figure 8(b)) with a slightly more anisotropic orientational distribution of the angular velocity for more elongated particles. Instead, the correlation between angular velocity fluctuations and local orientation seems independent of the applied confinement (see figure 8(a)).

To shed some light on the role of the shape anisotropy of the particles on the correlation between particles orientation and rotation, we analyse the heterogeneity of the orientational angular velocity function ω'_θ. For this purpose, we define the dimensionless parameter χ:

$$\chi = \frac{1}{\pi\overline{\omega'_\theta}}\int_{-\pi/2}^{\pi/2} |\omega'_\theta - \overline{\omega'_\theta}| \ \mathrm{d}\theta, \tag{3}$$

where $\overline{\omega'_\theta}$ represents the average value of the ω'_θ function. The parameter χ quantifies the deviation of the ω'_θ function from its mean value $\overline{\omega'_\theta}$. Therefore the parameter χ increases with the heterogeneity of ω'_θ, and so the higher the value of χ the stronger is the correlation between θ and ω. For the case of isotropic particles the angular velocity is not correlated to the orientation and the function ω'_θ has a constant value equal to 0.5 (since $\omega = -\dot{\gamma}/2$), and therefore the parameter χ is equal to zero.

The mean value of the ω'_θ function, obtained for the experimental combinations here considered, is displayed in figure 8(c). It is interesting to note that, even if rotations are strongly inhibited when increasing the particles' elongation (see figure 5), we observe that the mean value of the ω'_θ function assumes an approximately constant value independently of the particles' aspect ratio. The fact that the average value of the bin average angular velocity $\overline{\omega'_\theta}$ is different from the average angular velocity $\overline{\omega'}$ is not surprising because the particle orientation distribution is not uniform. Particles spend more time being aligned with their preferred direction, which is also that characterised by the slowest angular velocity, and therefore $\overline{\omega'} < \overline{\omega'_\theta}$. It is however quite surprising that $\overline{\omega'_\theta}$ has an approximately constant value, independently of the particles elongation.

From the experimental results we note a monotonic increase of the parameter χ with the shape anisotropy of the particles (see figure 8(d)). Thus, the heterogeneity of the ω'_θ function grows with the particle elongation, revealing that the correlation between local particle orientation and angular velocity is magnified when increasing the aspect ratio of the particles. Negligible differences in the value of χ are instead observed when changing the vertical load (see figure 8(d)), thus confirming that the correlation between angular velocity and local particle orientation is independent of the applied confinement.

In the light of the obtained results, one can note that the angular dependence of the rotation rate of the particles observed in our system is qualitatively in agreement with the model of Jeffery [33], even if the latter refers to a completely different system (i.e. dynamics of an isolated ellipsoidal particle in a viscous flow). In fact, in both cases particles' angular velocity increases with the misalignment with the preferential orientation (the flow direction in Jeffery's model), and this effect becomes stronger as the particles' aspect ratio increases thus leading to an increase of the heterogeneity of the ω'_θ function. Moreover, the constancy of the mean value of the ω'_θ function, independently of the particles' aspect ratio (see figure 8(c)), seems to represent another common feature of our granular system and the Jeffery's model. We can therefore state that also in our granular system the heterogeneity of the orientational distribution of the angular velocity can be related to a balance between the rotation induced by flow vorticity and the proneness of particles to assume a preferential orientation. Nevertheless, Jeffery's model does not correctly describe the behaviour of elongated particles in our granular flow from several points of view. Firstly, Jeffery's model does not predict

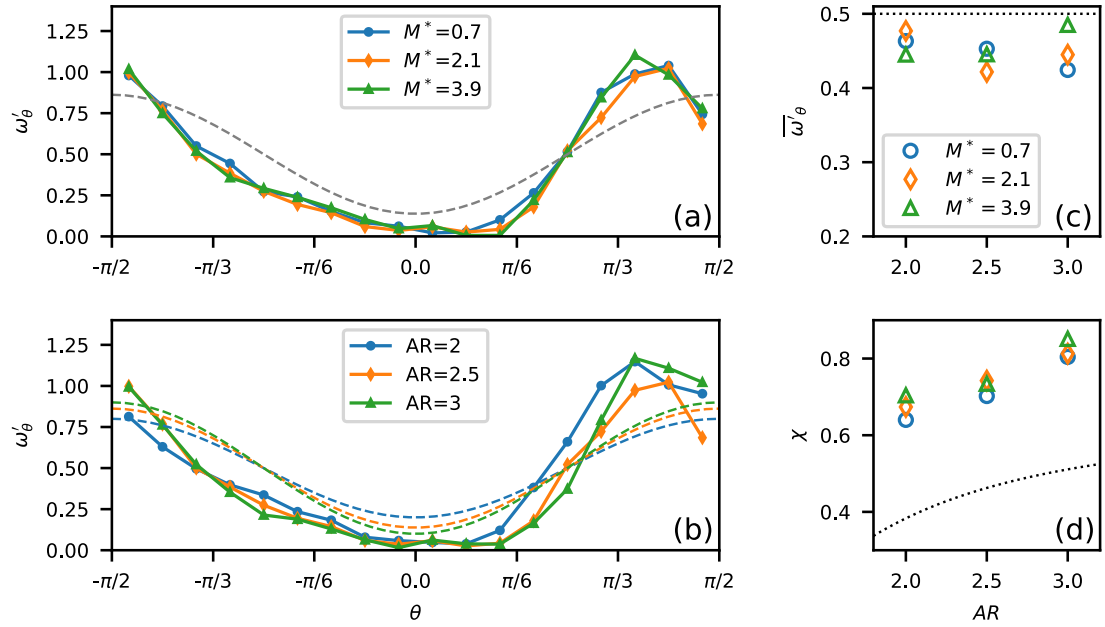

Figure 8. Normalised average particles angular velocity ω'_θ as a function of the particles' orientation: (a) effect of the vertical load M^* (AR = 2.5), (b) effect of the aspect ratio AR ($M^* = 2.1$). The dashed lines refer to Jeffery's model [33]. (c) Mean value of the ω'_θ function and (d) parameter χ as a function of the particles' aspect ratio (same legend as figure 8(c)). The black-dotted line represents the values obtained from the Jeffery's model [33].

the misalignment of the average particle orientation with respect to the flow direction. Secondly, the heterogeneity is more pronounced in our granular flow as shown by the higher values of the parameter χ obtained in our experiments than the one predicted by the Jeffery's model (black-dotted line in figure 8(d)). Thirdly, in our case the function ω'_θ is not symmetric with respect to θ_{av}, similarly to the experimental observation presented by Börzsönyi *et al* [24].

As observed in previous studies [24, 27], the above discussed differences from the Jeffery's model arise from the 'granular' nature of the system. In fact, differently from the case of an isolated particle in a viscous flow, in a granular medium particles are entangled with neighbours. On the one hand this induces a stronger geometrical frustration to the particles' rotation (other than the frustration deriving from the shape anisotropy of the particle itself), on the other hand it increases the tendency of particles to assume a preferential orientation with respect to the flow direction. Both of these phenomena reflect in a strengthening of the orientational dependence of the particles' angular velocity. It should be noted that, in our case, the asymmetry of the distribution of the angular velocity with θ, and so the deviation from the Jeffery's model, are more marked than what has been observed in the free surface flow of [24]. This can be ascribed to the highly confined nature of our flow configuration in which the coupling of shear and dilation can be very important.

6. Conclusions

In this work we discuss the first—to our knowledge—detailed experimental study of rotational dynamics of elongated particles in a fully confined shear flow. This configuration is characterised by shear localisation and therefore allows one to study the joint effect of vertical confinement and shear heterogeneity on rotational dynamics and orientational ordering.

The flow is characterised by an exponential velocity profile, which decay is controlled by the applied confinement. Interestingly, the translational velocity profile was found to be only slightly dependent on the particle shape, which means that the shear heterogeneity was equivalent for the particle types studied.

A first important result was found concerning the time-averaged angular velocity of the particles. While the translational velocity was found to be nearly unaffected by the particle shape, the angular velocity is instead significantly influenced by the particles elongation: longer particles are more frustrated by the surrounding ones and rotate less in average. The more elongated the particle, the larger the deviation of the angular velocity from the vorticity of the flow.

The shear heterogeneity was found to influence both the rotational dynamics of the grains and the orientational order. Again, the most important effect was observed on the average angular velocity of the

grains. The angular velocity, normalised by the shear rate, was observed to systematically decrease with the shear rate, which means that the deviation from the flow vorticity was higher in the low shear rate regions. This proves that, the proneness of an elongated particle to rotate is clearly shear rate dependent, and thus that flow heterogeneity affects the particle rotation dynamics. Such a shear-rate dependent inhibition of particles rotations was not reported in previous works on free surface flows [23, 24], and therefore may be a remarkable characteristic of confined granular flows. We suggest that this behaviour is related to local differences in the solid fraction. The medium is expected to be less dense in regions at higher shear rate, therefore the rotation is less frustrated due to the weaker particles' entanglement in such regions. A less pronounced effect of flow heterogeneity was instead observed in the orientational order of the granular system, with the emergence of slightly more ordered states in region characterised by lower shear rates. Remarkably, the rotational dynamics and the orientational order were found to be independent of the applied confinement.

Then, in order to try to better understand the particle rotation dynamics, we focused on the particle-scale, by analysing the correlation between angular velocity fluctuations and local particle orientation. For this purpose, we studied the function ω'_θ which quantifies the correlation between the angular velocity, bin-averaged with respect to the particle orientation, and the particle orientation itself. On an average basis, ω'_θ shows a minimum when particles are oriented closer to θ_{av}, while ω'_θ is maximum when they are oriented perpendicularly to θ_{av}. Surprisingly, we found that the mean value of the ω'_θ function has an approximately constant value independently of the particles aspect ratio. The heterogeneity of the ω'_θ function increases with the particles aspect ratio denoting a stronger correlation between rotations and orientation for more elongated particles. Conversely, the ω'_θ function seems independent of the applied confinement. The orientational order was found to systematically increase with the heterogeneity of ω'_θ (i.e. χ parameter), which agrees with the hypothesis that orientational ordering is caused by the correlation between angular velocity fluctuations and local particle orientation. The correlation between angular velocity fluctuations and local particle orientation seems to play a crucial role on the behaviour of granular flows made of elongated particles. This correlation is non-trivial and represents an interesting subject for further investigations.

Acknowledgments

Authors AP and FG acknowledge the financial support of Cariverona R & S 2018 and MIUR (Redreef—PRIN 2017 Call, Prot. 2017YPMBWJ). Authors AP, RA and PR acknowledge financial support from ANR (ANR-20-CE08-0028 MoNoCoCo).

Conflict of interest

There are no conflicts to declare.

Data availability statement

The data that support the findings of this study are available upon reasonable request from the authors.

ORCID iDs

Antonio Pol https://orcid.org/0000-0001-6368-7194
Riccardo Artoni https://orcid.org/0000-0001-9757-4489
Patrick Richard https://orcid.org/0000-0003-2380-6552

References

[1] Torquato S and Stillinger F H 2010 *Rev. Mod. Phys.* **82** 2633–72
[2] Donev A, Cisse I, Sachs D, Variano E A, Stillinger F H, Connelly R, Torquato S and Chaikin P M 2004 *Science* **303** 990–3
[3] Olson C J, Reichhardt C, Mccloskey M and Zieve R J 2002 *Europhys. Lett.* **57** 904–10
[4] Antony S J and Kuhn M R 2004 *Int. J. Solids Struct.* **41** 5863–70
[5] Zuriguel I, Mullin T and Rotter J M 2007 *Phys. Rev. Lett.* **98** 028001
[6] Hidalgo R C, Zuriguel I, Maza D and Pagonabarraga I 2009 *Phys. Rev. Lett.* **103** 118001
[7] Hidalgo R C, Zuriguel I, Maza D and Pagonabarraga I 2010 *J. Stat. Mech.* 06025
[8] Kanzaki Cabrera T, Acevedo Escalante M, Zuriguel I, Pagonabarraga I, Maza D and Hidalgo R 2011 *Eur. Phys. J.* E **34** 1–8

[9] Blouwolff J and Fraden S 2006 *Europhys. Lett.* **76** 1095–101
[10] Mailman M, Schreck C F, O'Hern C S and Chakraborty B 2009 *Phys. Rev. Lett.* **102** 255501
[11] Schreck C F, Xu N and O'Hern C S 2010 *Soft Matter* **6** 2960–9
[12] Villarruel F X, Lauderdale B E, Mueth D M and Jaeger H M 2000 *Phys. Rev.* E **61** 6914–21
[13] Lumay G and Vandewalle N 2004 *Phys. Rev.* E **70** 051314
[14] Ribière P, Richard P, Delannay R and Bideau D 2005 *Phys. Rev.* E **71** 011304
[15] Ribière P, Richard P, Bideau D and Delannay R 2005 *Eur. Phys. J.* E **16** 415–20
[16] Lumay G and Vandewalle N 2006 *Phys. Rev.* E **74** 021301
[17] Azéma E and Radjaï F 2010 *Phys. Rev.* E **81** 051304
[18] Guo Y, Wassgren C, Hancock B, Ketterhagen W and Curtis J 2013 *Phys. Fluids* **25** 063304
[19] Nagy D B, Claudin P, Börzsönyi T and Somfai E 2017 *Phys. Rev.* E **96** 062903
[20] Börzsönyi T and Stannarius R 2013 *Soft Matter* **9** 7401–18
[21] Reddy K A, Kumaran V and Talbot J 2009 *Phys. Rev.* E **80** 031304
[22] Campbell C S 2011 *Phys. Fluids* **23** 013306
[23] Börzsönyi T, Szabó B, Törös G, Wegner S, Török J, Somfai E, Bien T and Stannarius R 2012 *Phys. Rev. Lett.* **108** 228302
[24] Börzsönyi T, Szabó B, Wegner S, Harth K, Török J, Somfai E, Bien T and Stannarius R 2012 *Phys. Rev.* E **86** 051304
[25] Mandal S and Khakhar D V 2016 *Phys. Fluids* **28** 103301
[26] Trulsson M 2018 *J. Fluid Mech.* **849** 718–40
[27] Artoni R and Richard P 2019 *Acta Mech.* **230** 3055–69
[28] Hidalgo R C, Szabó B, Gillemot K, Börzsönyi T and Weinhart T 2018 *Phys. Rev. Fluids* **3** 074301
[29] Börzsönyi T, Somfai E, Szabó B, Wegner S, Mier P, Rose G and Stannarius R 2016 *New J. Phys.* **18** 093017
[30] Tang J and Behringer R P 2016 *Europhys. Lett.* **114** 34002
[31] Ashour A, Wegner S, Trittel T, Börzsönyi T and Stannarius R 2017 *Soft Matter* **13** 402–14
[32] To K, Mo Y K, Pongó T and Börzsönyi T 2021 *Phys. Rev.* E **103** 062905
[33] Jeffery G B 1922 *Proc. R. Soc. London* A **102** 161–79
[34] Artoni R and Richard P 2015 *Phys. Rev. Lett.* **115** 158001
[35] Artoni R, Soligo A, Paul J-M and Richard P 2018 *J. Fluid Mech.* **849** 395–418
[36] Richard P, Artoni R, Valance A and Delannay R 2020 *Granular Matter* **22** 81
[37] Tirapelle M, Santomaso A C, Richard P and Artoni R 2021 *Adv. Powder Technol.* **32** 1305–17
[38] Lun C K K and Bent A A 1994 *J. Fluid Mech.* **258** 335–53
[39] Prochnow M 2012 Ecoulements denses de grains secs *PhD Thesis* Ecole des Ponts ParisTech
[40] da Cruz F, Emam S, Prochnow M, Roux J N and Chevoir F m c 2005 *Phys. Rev.* E **72** 021309
[41] Koval G, Roux J N, Corfdir A and Chevoir F m c 2009 *Phys. Rev.* E **79** 021306
[42] Azéma E, Descantes Y, Roquet N, Roux J N and Chevoir F m c 2012 *Phys. Rev.* E **86** 031303
[43] Nagy D B, Claudin P, Börzsönyi T and Somfai E 2020 *New J. Phys.* **22** 073008
[44] Berzi D, Thai-Quang N, Guo Y and Curtis J 2016 *Phys. Rev.* E **93** 040901
[45] Marschall T, Keta Y-E, Olsson P and Teitel S 2019 *Phys. Rev. Lett.* **122** 188002